

## Article

# Experimental and Numerical Investigation of Shear Strengthening of Simply Supported Deep Beams Incorporating Stainless Steel Plates

Ahmed Hamoda <sup>1</sup>, Saad A. Yehia <sup>2</sup>, Mizan Ahmed <sup>3,\*</sup>, Khaled Sennah <sup>4</sup>, Aref A. Abadel <sup>5</sup>  
and Ramy I. Shahin <sup>2</sup>

- <sup>1</sup> Civil Engineering Department, Faculty of Engineering, Kafrelsheikh University, Kafrelsheikh 6860404, Egypt; ahmed\_hamoda@eng.kfs.edu.eg
- <sup>2</sup> Department of Civil Engineering, Higher Institute of Engineering and Technology, Kafrelsheikh 6860404, Egypt; saad\_yehia@kfs-hiet.edu.eg (S.A.Y.); ramy.shahin@kfs-hiet.edu.eg (R.I.S.)
- <sup>3</sup> Centre for Infrastructure Monitoring and Protection, School of Civil and Mechanical Engineering, Curtin University, Kent Street, Bentley, WA 6102, Australia
- <sup>4</sup> Department of Civil Engineering, Toronto Metropolitan University, Toronto, ON M5B 2K3, Canada; ksennah@torontomu.ca
- <sup>5</sup> Department of Civil Engineering, College of Engineering, King Saud University, Riyadh 11421, Saudi Arabia; aabadel@ksu.edu.sa
- \* Correspondence: mizan.ahmed@curtin.edu.au

**Abstract:** In this study, the effectiveness was investigated of shear strengthening techniques in reinforced concrete (RC) deep beams incorporating stainless steel plates (SSPs). Four RC deep beams were tested under incremental static loading until failure to examine the proposed strengthening techniques. The key parameters considered in this study included the arrangement of the externally bonded SSPs. The experimental findings demonstrated that strengthening using SSPs led to substantial improvements in their performance compared to the unstrengthened control beam. The use of SSPs increased the ultimate shear capacity by 129 to 175% over the control specimen. Finite element models (FEMs) were developed to simulate the responses of the tested beams strengthened using SSPs. Parametric studies were then conducted using the validated FEM to investigate to identify the effects of the area of SSPs on the shear capacity of the beams. The parametric studies concluded that increasing the plate thickness resulted in the enhanced shear capacity of the deep beam specimens up to a critical point upon which the increases in the thickness have insignificant effects on the shear strength. The accuracy of the design equations given by European and American codes in predicting the shear strength of the deep beams is examined.

**Keywords:** deep beams; shear strengthening; stainless steel plates; finite element analysis



**Citation:** Hamoda, A.; Yehia, S.A.; Ahmed, M.; Sennah, K.; Abadel, A.A.; Shahin, R.I. Experimental and Numerical Investigation of Shear Strengthening of Simply Supported Deep Beams Incorporating Stainless Steel Plates. *Buildings* **2024**, *14*, 3680. <https://doi.org/10.3390/buildings14113680>

Academic Editor: Francesca Ferretti

Received: 12 October 2024

Revised: 12 November 2024

Accepted: 18 November 2024

Published: 19 November 2024



**Copyright:** © 2024 by the authors. Licensee MDPI, Basel, Switzerland. This article is an open access article distributed under the terms and conditions of the Creative Commons Attribution (CC BY) license (<https://creativecommons.org/licenses/by/4.0/>).

## 1. Introduction

Widely employed in critical infrastructure like high-rise buildings, bridges, and foundations, reinforced concrete (RC) deep beams serve as crucial load-bearing elements. Their shear span-to-depth ratio ( $a/d$ ) of equal or less than 2.5 distinguishes them from slender beams, leading to more complicated deformation patterns under heavy loads [1]. Recognizing this unique behavior, researchers have explored their shear response through numerous experiments [2–4] and theoretical models [5–9]. Unlike the flexural and flexural shear failures shown in Figures 1a and 1b, respectively, the initiation of shear cracks at mid-depth in deep beams poses unique challenges for design due to their brittle nature and outward growth [10]. Their large depth makes them susceptible to shear failure due to the diagonal splitting, as seen in Figure 1c [11]. In addition, a significant portion of the civil infrastructure network, burdened by ever-increasing operational demands, harsh

environmental exposures, inherent construction flaws, and a history of insufficient maintenance, desperately needs rehabilitation or reinforcement interventions [12]. External shear strengthening enhances the shear resistance, delays the onset of diagonal cracking, reduces crack widths, and increases the ultimate shear strength [13].

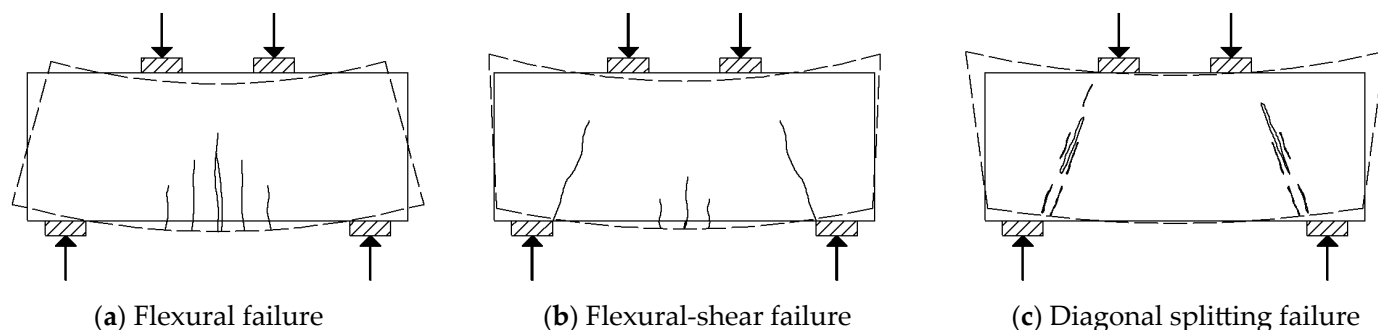


**Figure 1.** Failure modes of deep beams.

The external bonding reinforcement (EBR) technique utilizing steel plates was first explored by L’Hermite, who studied the steel–epoxy–concrete interface [14]. Since then, numerous investigations have characterized the bond behavior of strengthening elements using EBR [15–23]. Hamoda et al. [24] examined the effectiveness of using hybrid SHCC-mesh in the shear strengthening of deep beams. The effects of glass fiber mesh and steel wire mesh as well as the number of layers of mesh were examined. The proposed EBR technique significantly improved the shear performance of the deep beams. Fiber-reinforced polymer (FRP) composites are used for the strengthening of concrete [25–27]. Abadel et al. [28] examined the effectiveness of carbon fiber-reinforced polymer (CFRP) strips in shear strengthening of deep beams with or without ultra-high-performance concrete (UHPC). Test results showed that applications of UHPC with CFRP sheets remarkably enhanced the shear strength of deep beams. Similar conclusions were drawn by Ahmad et al. [29].

Strengthening using stainless steel plates (SSPs) offers advantages compared to mild steel or FRP composites. Compared to mild steel, stainless steel exhibits superior durability due to its excellent corrosion resistance. Also, stainless steel displays ductile response, a critical factor favoring its selection over FRP for strengthening structures [30]. Furthermore, previous research has shown that the position of SSPs, e.g., in an inclined, vertical, or horizontal configuration, affects the strengthening behavior of RC beams. In this study, the use is proposed of SSPs for shear strengthening of simply supported RC deep beams that are subjected to harsh weather and require adaptation of corrosion resistance materials for durability purposes. However, there has not been any study performed to study the application of SSPs for the shear strengthening of deep beams. Based on the research gaps, the specific aims of this study are to study the effects of the arrangement of the externally bonded SSPs in horizontal, vertical, and inclined positions on the shear strength of RC deep beams. Nonlinear finite element models (FEMs) were also developed to simulate the response of the tested beams strengthened using SSPs. Followed by the validation of the FEMs, parametric studies were carried out to examine the effects of the thickness of the SSPs on the shear capacity. Moreover, the accuracy of the design equations given by Eurocode 2 [31] and ACI-318-19 [32] in predicting the shear strength of the deep beams is evaluated.

## 2. Materials and Methods

### 2.1. Details of the Tested Beams

The testing of the beams included one unstrengthened control deep beam, and three RC deep beams strengthened by SSPs bonded in horizontal, vertical, and inclined positions. All the beams possessed identical reinforcement arrangements and dimensions, namely, 150 mm wide, 400 mm deep, and 750 mm long. Figure 2 illustrates the details of the tested

beams' reinforcement arrangements and strengthening techniques. As shown in Figure 2a, 16 mm and 12 mm diameter bars were used as the tension and compression reinforcements, respectively. The beams were designed so that they primarily failed in shear. For this, stirrups of 8 mm diameter at 100 mm spacing were provided in all beams but at the critical shear zone, a greater spacing of 150 mm was adopted that provided a smaller ratio to create a weak shear region to be strengthened with the proposed strengthening techniques. The full covering of the critical shear zone with the SSPs will result in the improvement of the strength of the shear strength of such a beam. However, as reported by Hamoda et al. [19], utilization of the full covering of the critical shear zone with a single stainless steel sheet in RC beams resulted in only a 3% and 10% increase in the strength of ultimate strength compared to the strips of SSPs positioned in vertical and inclined positions. To ensure the most cost-effective method, the authors proposed strengthening RC deep beams using strips of SSPs rather than covering the whole area of the critical shear zone with a single stainless steel sheet. The selection of the size of the strip of the SSPs was based on the preliminary finite element model to ensure the most cost-effective solution for the shear strengthening of the RC deep beams. As seen in Table 1, beam B0 is the unstrengthened master beam whereas B-SS-H, B-SS-V, and B-SS-I beams were externally strengthened with bonded SSPs in different arrangements, as follows: (a) horizontal, (b) vertical, and (c) inclined, as depicted in Figure 2b, Figure 2c, and Figure 2d, respectively. The horizontal and inclined SSPs measured 377 mm × 40 mm, spaced at 45 mm intervals (3 strips total, as shown in Figure 2b,d). Their orientation was perpendicular to the expected principal crack in beam B0. However, the middle strip of specimen B-SS-I was increased slightly by 68 mm compared to other two strips (445 mm is total length) as it countered the issue of anchoring the bolts while hitting the vertical strips when using the same length of strips as the two adjacent strips. However, as the preliminary study carried out using FEM shows, this slight additional length of SSPs has negligible effects when compared with the results of the beam with all three same strip lengths. The vertical SSPs were also 377 mm × 40 mm, with 45 mm spacing between them (three strips in total, Figure 2c).

**Table 1.** Test matrix and details of beam groups.

Beam ID	Identical Details			Shear Reinforcement	Configuration of Strengthening
	Beam Geometry (mm)	Reinforcement	Type of Strengthening		
B0 [24]	Height = 400 Width = 150 length = 750	Upper = 2-D12	Externally bonded reinforcement (EBR)	No reinforcement	---
B-SS-H		Lower = 3-D16		EBR with stainless steel strengthening	Horizontal strips
B-SS-V		Stirrups = 8 mm			Vertical strips
B-SS-I		(see Figure 2a)			Inclined strips

## 2.2. Material Properties

Normal-strength concrete (NC) with the mix design given in Table 2 was used to cast the beams. Standard cylinders (150 × 300 mm) were cast to measure the compressive strength of concrete and listed in Table 2. The tensile strength given in Table 2 was measured using direct tensile testing. The sample cylinders were cured identically as the tested beams. The compression tests of the concrete materials were carried out according to ASTM C39/C39M [33]. The material properties of steel elements were obtained from tensile coupon tests as shown in Figure 3, with experimental results shown in Table 3. The stress–strain curves of the steel elements obtained from the tensile tests are given in Figure 4.

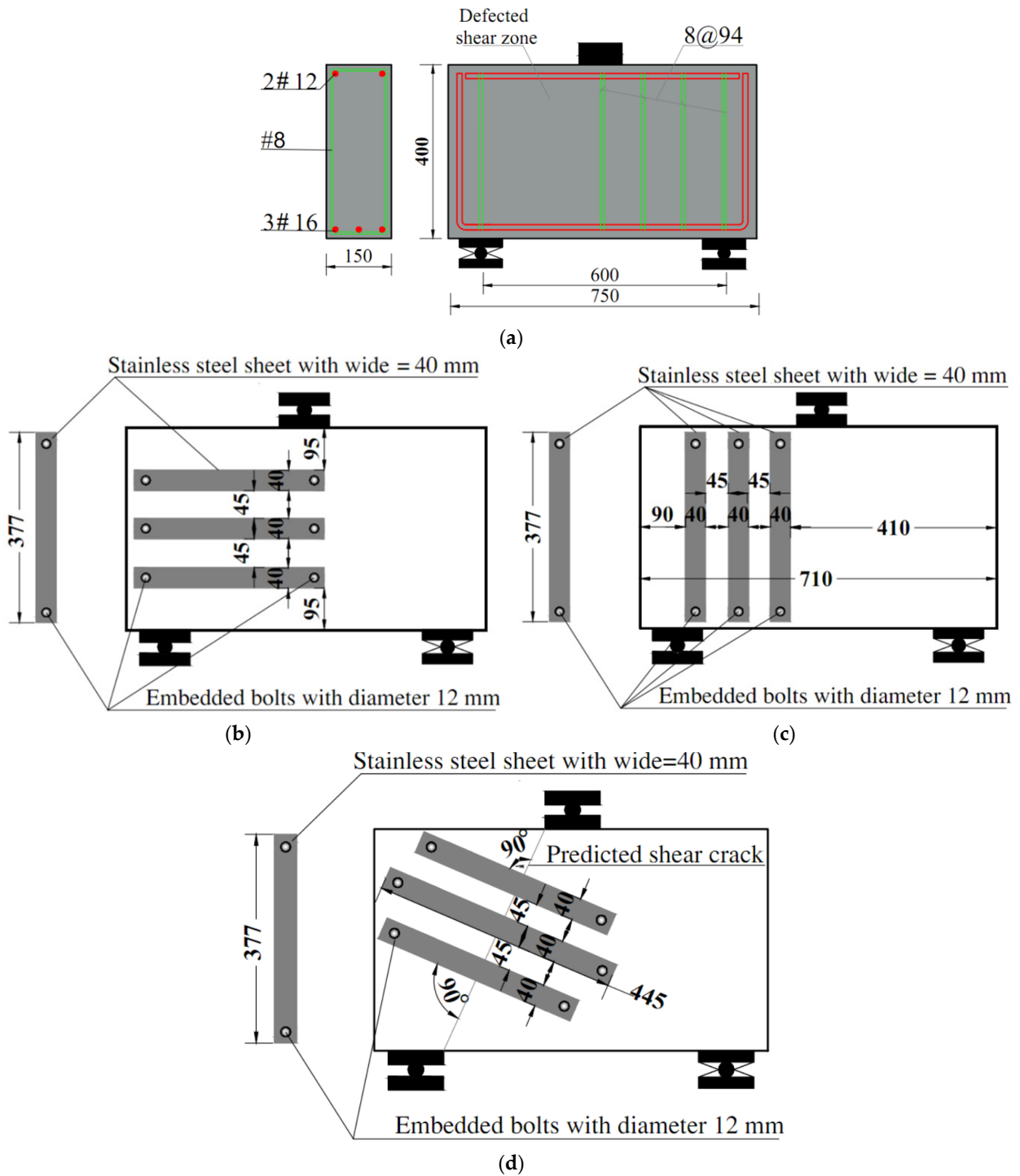


**Figure 2.** General details for reinforcement and strengthening: (a) reinforcement for defected beam used for strengthening; (b) beam B-SS-H; (c) beam B-SS-V; (d) beam B-SS-I.

**Table 2.** Concrete mix design and properties.

Concrete	Cement (kg/m <sup>3</sup> )	Fine Aggregate (kg/m <sup>3</sup> )	Coarse Aggregate (kg/m <sup>3</sup> )	Water/ Cement Ratio	Compressive Strength $f_c'$ (MPa)	Tensile Strength $f_{ct}'$ (MPa)	Elastic Modulus (MPa)
NC	350	700	1150	0.43	32	2.12	19,800



Figure 3. Tensile coupon test of a typical stainless steel plate specimen.

Table 3. Mechanical properties of steel.

Element	The Function of Steel Element	Yielding Stage		Ultimate Stage		E (GPa)	Poisson's Ratio
		$\sigma_y$ (MPa)	$\epsilon_y$ (%)	$\sigma_u$ (MPa)	$\epsilon_u$ (%)		
8 mm	Stirrups	295	0.154	453	13.1	191	0.3
12 mm	Compression steel bar	364	0.176	529	12.23	206	0.3
16 mm	Tension steel bar	367	0.175	551	13.93	209	0.3
SSPs	EBR strengthening	306	0.145	441	11.01	211	0.3

Note: SSPs: stainless steel plates; EBR: external bonding reinforcement;  $\sigma$ : stress;  $\epsilon$ : strain; E: modulus of elasticity.

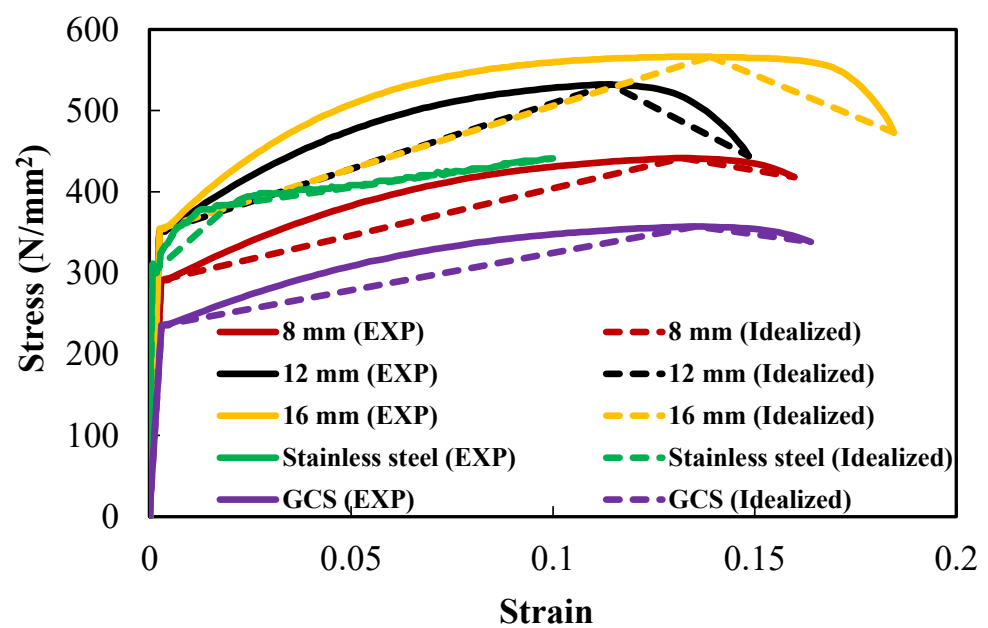
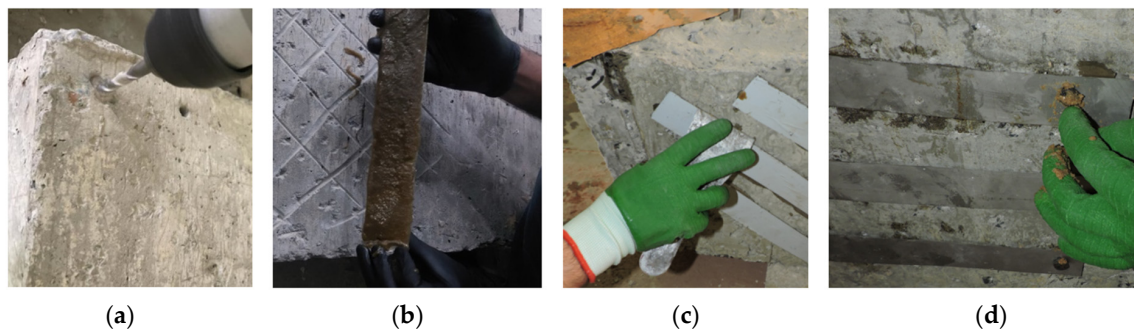


Figure 4. Stress–strain curves of steel elements.

### 2.3. Beam Specimen Preparation

The beams were first cast using wooden formworks. Once the formwork was prepared, the reinforcing cages consisting of flexural reinforcement bars and stirrups were placed inside and the concrete was poured. In order to strip the formwork easily, grease was applied inside the formwork prior to casting concrete. A vibrator was used for the compaction during the casting. After 24 h of casting, the formworks were striped and the beams were left to air-cure for 28 days. After 28 days of concrete curing, the beams were strengthened using SSPs on both sides of the strengthened zone. To enable complete contact between SSPs and the concrete surface in the shear zone, 16 mm diameter holes were drilled on both ends of the SSPs to bolt them on both sides of the beam, as depicted in Figure 5a. Then, the SSPs were bonded using Sikadur 31 epoxy adhesive, as shown in Figure 5b,c. Post-installed anchor bolts of 12 mm diameter were used to secure the SSPs after filling the holes partially with epoxy (Figure 5d).



**Figure 5.** Strengthening using SSPs: (a) drilling bolt holes; (b) application of chemical epoxy; (c) bonding of SSPs; (d) installing anchor bolts.

### 2.4. Test Instrumentation

The load was applied using a testing machine with a capacity of 2500 kN. Figure 6 shows the setup of the test program. Before testing, the beams were cleaned to remove dust and coated with white paint to improve visibility for identifying cracks during testing. Each beam was supported over hinged support at one end and roller support at the other, having an effective span of 600 mm. A load was applied in the middle, as shown in Figure 6a [24]. A linear variable displacement transducer (LVDT) was used to measure the vertical deflection at the load point which is located at the mid-span of the beam. PI-shape displacement transducer was installed at the expected shear zone to record tensile strain. The beams were gradually loaded with 2.00 kN increments until failure. Just before the failure, the LVDT was disengaged.

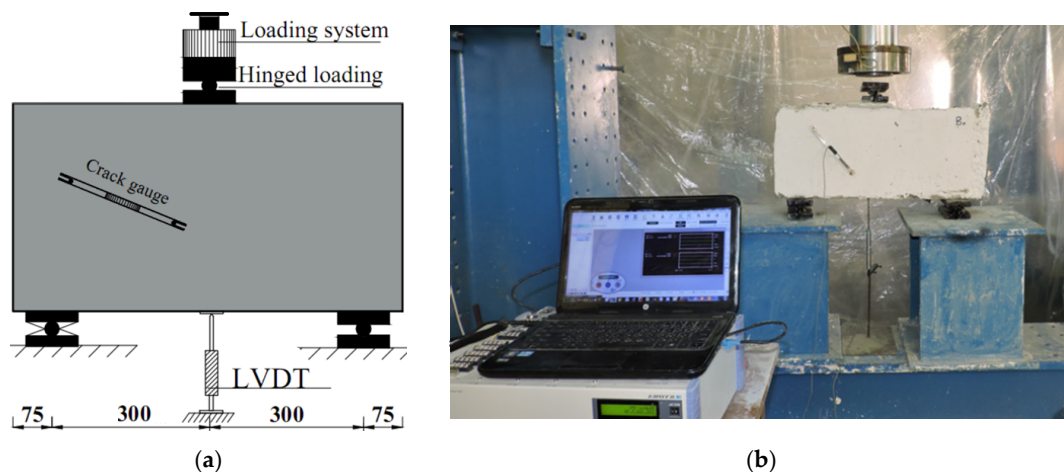


**Figure 6.** Test setup: (a) schematic diagram; (b) picture of the test set-up.

### 3. Discussions on the Test Results

The initial cracking loads, crack patterns, failure modes, ultimate shear capacities, and load–deflection responses were measured and the corresponding elastic stiffnesses and energy absorption capacities are listed in Tables 4 and 5. The elastic stiffness was determined from the initial elastic slope of the load–displacement curves, while the absorbed energy of the beams was computed by evaluating the area under the load–deflection curves [34,35].

**Table 4.** Loads and deflections of the tested beams.

Specimen ID	Ultimate Stage		
	$P_u$ (kN)	$P_{uB}/P_{uB0}$	$\Delta_{Pu}$ (mm)
B0	85.32	1.00	7.79
B-SS-H	210	2.46	2.75
B-SS-V	195	2.29	6.71
B-SS-I	235	2.75	11.37

**Table 5.** Failure mode, absorbed energy, and elastic stiffness of the tested beams.

Specimen's ID	Elastic Stiffness (K)		Absorbed Energy (AE)		Failure Mode
	K (kN/mm)	$K_B/K_{B0}$	AE (kN.mm)	$AE_B/AE_{B0}$	
B0	18.71	1.00	344.54	1.00	S
B-SS-H	176	9.41	1215	3.53	S then B
B-SS-V	51	2.73	1979	5.74	S then B
B-SS-I	63	3.37	3419	9.92	S

Note: S: shear failure; B: bearing close to the support; F: flexural failure.

#### 3.1. Cracking Pattern and Failure Modes

Figure 7 presents the cracking patterns and failure modes observed during testing. For beam B0, visible initial hairline cracks originated diagonally from the loading plate toward the support at 28.25 kN load which is about 33% of its ultimate load ( $P_u$ ). With increasing the applied load, the shear crack progressively widened, with more minor secondary cracks appearing, as depicted in Figure 7a. Significantly wider shear cracks formed along the strut from the loading plate edge to the support when the applied load reached its ultimate value of 85.32 kN.

For the beams strengthened in the critical shear span using various SSP configurations, hairline cracks gradually emerged during loading until failure. Shear cracks were initiated and propagated under the SSPs, leading to failure due to a major shear crack followed by concrete bearing failure at the support at ultimate load, as depicted in Figure 7b,c for beams B-SS-H, and B-SS-V, respectively. However, strengthened with SSPs configured horizontally exhibited fewer cracks than the beam strengthened with SSPs configured vertically which resulted in the higher cracking and ultimate load. Moreover, beam B-SS-I with diagonal SSPs exhibited a major shear–flexural crack at failure, as depicted in Figure 7d. Initial diagonal cracks occurred at approximately 160 kN (76% of  $P_u$ ) for B-SS-H, 108 kN (55% of  $P_u$ ) for B-SS-V, and 171 kN (73% of  $P_u$ ) for B-SS-I. Nonetheless, when looking at the failure modes of the specimens, it was observed that the SSPs bent at their ultimate failure modes resulting in the loss of adhesion for specimen B-SS-H which experienced the rupture of SSPs at the anchor bolt (see Figure 7b), yet all the strengthened beams exhibited higher cracking and ultimate load due to the delay in the initiation of major diagonal crack(s).



### 3.2. Ultimate Loads and Corresponding Deflection

The ultimate loads illustrated in Figure 8 and Table 4 show that all strengthened beams exhibited enhancement in their ultimate loads than B0. Specifically, the ultimate loads ( $P_u$ ) increased by 146%, 129%, and 175% for B-SS-H, B-SS-V, and B-SS-I, respectively, compared to B0. One may observe that the B-SS-I beam with SSPs oriented diagonally exhibited the greatest cracking and ultimate loads compared to beams with vertical and horizontal SSP strengthening. Similarly, the deflection corresponding to the ultimate load also showed a similar trend for the strengthened beams where maximum deflection corresponding to the ultimate load was highest for B-SS-I followed by B-SS-V, and B-SS-H.

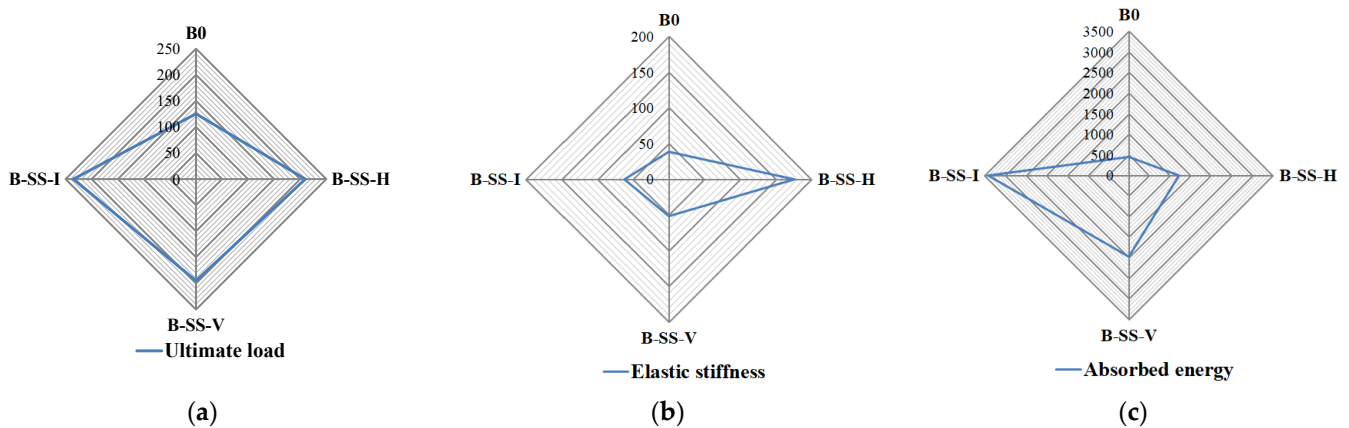


**Figure 8.** Comparison of test results; (a) ultimate load; (b) elastic stiffness; (c) absorbed energy.

### 3.3. Load–Deflection Curves

Figure 9 illustrates the load–deflection curves obtained during the tests. The load–deflection curves illustrate that the control beam B0 exhibited a linear response from zero loading until the cracking load, followed by a plastic zone before failing in shear. In contrast, all strengthened beams showed greater elastic stage and enhanced load-carrying capacities than B0. Table 4 reveals that the deflection at the ultimate load of beams strengthened with SSPs increased by 56% and 164% for beams B-SS-V and B-SS-I, respectively, compared to the control beam B0. Conversely, it decreased by 29% for beam B-SS-H. As depicted in Figure 9, various strengthening methods significantly influenced the beam deformation. One may observe that deflection results do not have a general trend since the failure modes of all beams were brittle shear failure.

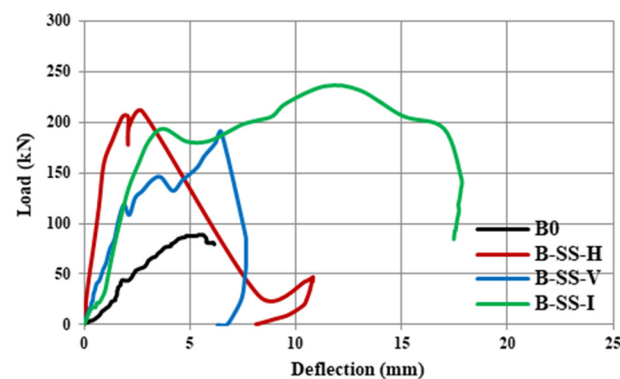


**Figure 9.** Load–deflection curves of tested specimens.

### 3.4. Elastic Stiffness and Absorbed Energy

Table 5 and Figure 8b,c display the calculated elastic stiffness and absorbed energy of the tested beams. Overall, applying various strengthening techniques resulted in a substantial enhancement in both absorbed energy and elastic stiffness for all specimens. Based on

the calculations, it was observed that the elastic stiffness of the specimens strengthened with SSPs improved by 841%, 173%, and 237% for beams B-SS-H, B-SS-V, and B-SS-I, respectively, compared to B0. As depicted in Figure 8c for the G1 group, the test results indicate that beam B-SS-I exhibited the most notable improvement in absorbed energy, followed by beams B-SS-V and B-SS-H, respectively. The enhancements of the energy absorption for B-SS-I, B-SS-V, and B-SS-H are calculated as 892%, 474%, and 253%, respectively.

#### 4. Numerical Simulation

The ABAQUS 14 software was employed for implementing the FEM. The predicted results were compared against the experimental observations to ensure the validity of the modeling.

##### 4.1. Material Modeling

The concrete damaged plasticity model (CDP) was adopted to simulate concrete's behavior. The CDP model stands out as a versatile tool, featuring components like tensile and compression damage, linked to tensile cracking, and relying on scalar plastic damage models. Trials were conducted to explore the sensitivity of the parameters of the CDP model. Based on the trials, the second stress invariant on the tensile to the compressive meridian ( $K_c$ ) was taken as 0.66, and the ratio of biaxial to uniaxial compressive yield stresses ( $f_{bo}/f_{co}$ ) was taken as 1.16. The dilation angle ( $\psi$ ), viscosity relaxation parameter ( $\mu$ ), and eccentricity ( $e$ ) were adopted as  $35^\circ$ , 0, and 0.1, respectively. Table 6 summarizes the CDP parameters used in the FEM.

**Table 6.** Summary of the CDP parameters used in the FEM.

Parameters	Value
The second stress invariant on the tensile to the compressive meridian ( $K_c$ )	0.66
The ratio of biaxial to uniaxial compressive yield stresses ( $f_{bo}/f_{co}$ )	1.16
dilation angle ( $\psi$ )	$35^\circ$
viscosity relaxation parameter ( $\mu$ )	0
eccentricity ( $e$ )	0.1

With regards to the stress–strain relationships of materials, Figure 4 illustrates the idealized uniaxial stress–strain curves of steel components adopted in this study. The compression stress–strain law was formulated using Carreira and Chu [36], as shown in Figure 10, and can be calculated using Equations (1)–(3). Additionally, the uniaxial tensile stress–strain behavior was taken as a linear behavior up to its tensile strain followed by linear descending to the ultimate strain.

$$f_c = f'_c \left[ \frac{\beta \left( \frac{\varepsilon_c}{\varepsilon_{c0}} \right)}{\beta - 1 + \left( \frac{\varepsilon_c}{\varepsilon_{c0}} \right)^\beta} \right] \quad (1)$$

$$f_t = \begin{cases} f_{tu} \left[ 1.2 \frac{\varepsilon_t}{\varepsilon_{t0}} - 0.2 \left( \frac{\varepsilon_t}{\varepsilon_{t0}} \right)^6 \right] & 0 \leq \varepsilon_t \leq \varepsilon_{t0} \\ f_{tu} \left[ \frac{\frac{\varepsilon_t}{\varepsilon_{t0}}}{1.25 \left( \frac{\varepsilon_t}{\varepsilon_{t0}} - 1 \right)^2 - \frac{\varepsilon_t}{\varepsilon_{t0}}} \right] & \varepsilon_{t0} \leq \varepsilon_t \end{cases} \quad (2)$$

where  $f_c$  and  $\varepsilon_c$  are the concrete longitudinal stress and the corresponding strain, respectively, and  $f'_c$  and  $\varepsilon_{c0}$  are the peak stress of concrete and the corresponding strain, respectively.  $\beta$  can be calculated using Equation (3).

$$\beta = \left( \frac{f'_c}{32.4} \right) + 1.55 \quad (3)$$

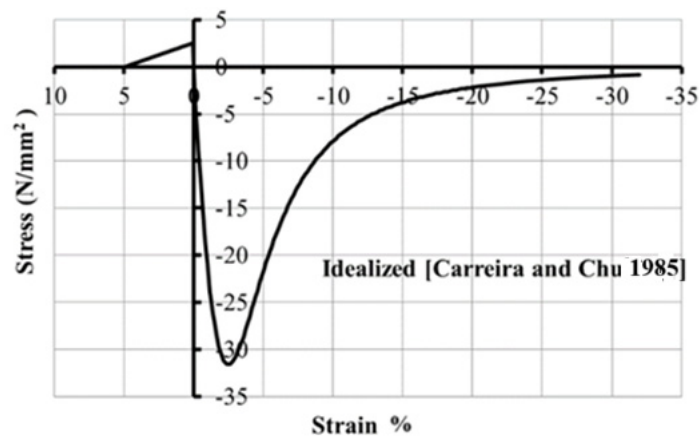


Figure 10. Stress–strain relationships of concrete [36].

#### 4.2. Mesh and Boundary Conditions

The FEM accurately replicated the exact details and specifications of the geometry, and boundary conditions of the tested beams. Eight-node linear hexahedral-reduced integration solid elements (C3D8R) were utilized to model the concrete element, loading plate, and supporting plates. As shown in Figure 11a, the longitudinal reinforcing steel bars and transverse steel stirrups were modeled using two-node linear 3D truss elements (T3D2). Additionally, four-node quadrilateral shell elements with reduced integration (S4R) were employed to simulate the response of the SSPs used for shear strengthening. A surface-to-surface contact interaction property represents the interface behavior between the NC and the SSPs, adopting hard contact in the normal direction and a penalty friction coefficient of 0.25 in the tangential direction [37,38]. The interaction between the concrete and the reinforcing steel bars and stirrups was modeled using embedded region constraints. After carrying out a sensitivity analysis, a mesh size of 20 mm was adopted for meshing.

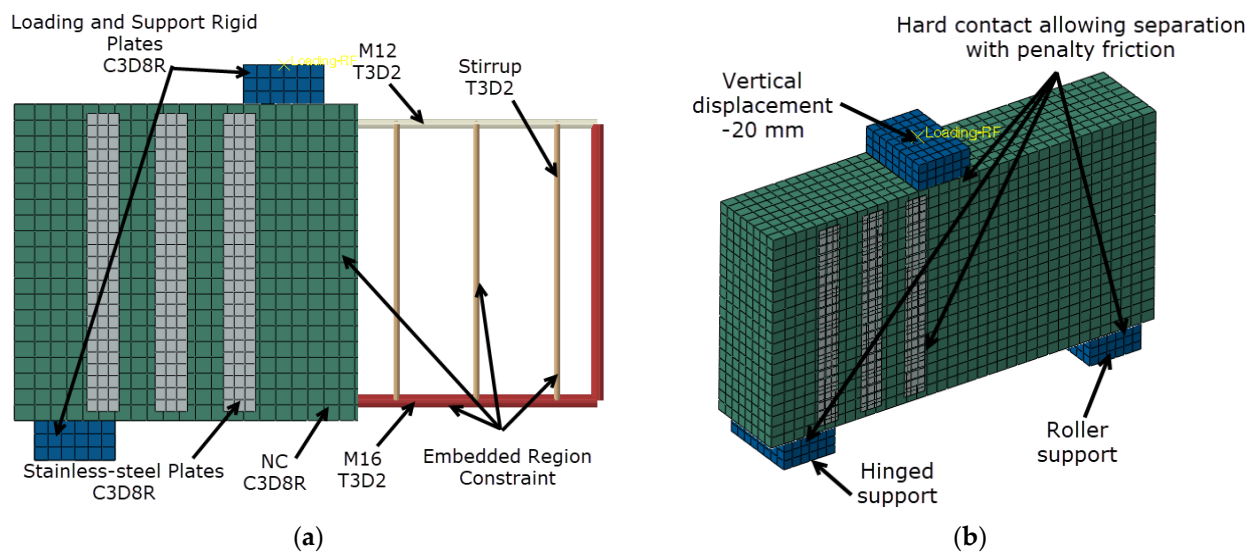


Figure 11. FEM modeling: (a) elevation and (b) isometric view.

The load was applied at a reference point of the upper loading plate beams, as depicted in Figure 11b. Similarly, the boundary conditions were applied at reference points at the supporting plates through coupling constraints.

## 5. Model Validation

The predicted results were compared with the experimental and failure modes, load–deflection curves, and ultimate loads for validation purposes. Figure 12 shows a close match between the test failure modes observed and those predicted by the FEM modeling. The FEM can capture the effect of beam strengthening using SSPs in improving the failure shape for the different specimens reasonably well. For example, as shown in the FEM prediction for B0, the diagonal shear stresses developed along a strut line between the loading plate and the support. Meanwhile, it can be noticed that the FEM predicted a shear–flexural failure for the specimen instead of the diagonal splitting that occurred in the control beam, which indicates that this type of strengthening is more effective than other methods.

Table 7 summarizes the numerical and experimental results, while Figure 12 depicts the comparisons of the load–deflection responses. The comparison between the actual and predicted FEM results demonstrates that the proposed finite element model can accurately predict the ultimate loads of the tested beams. The average ratio of FEM to experimental result is 1.01, with a corresponding CoV of 0.03. Furthermore, Figure 13 reveals a close agreement of the load–deflection responses up to the ultimate loads. Moreover, the FEM model can accurately capture the initial linear elastic response.

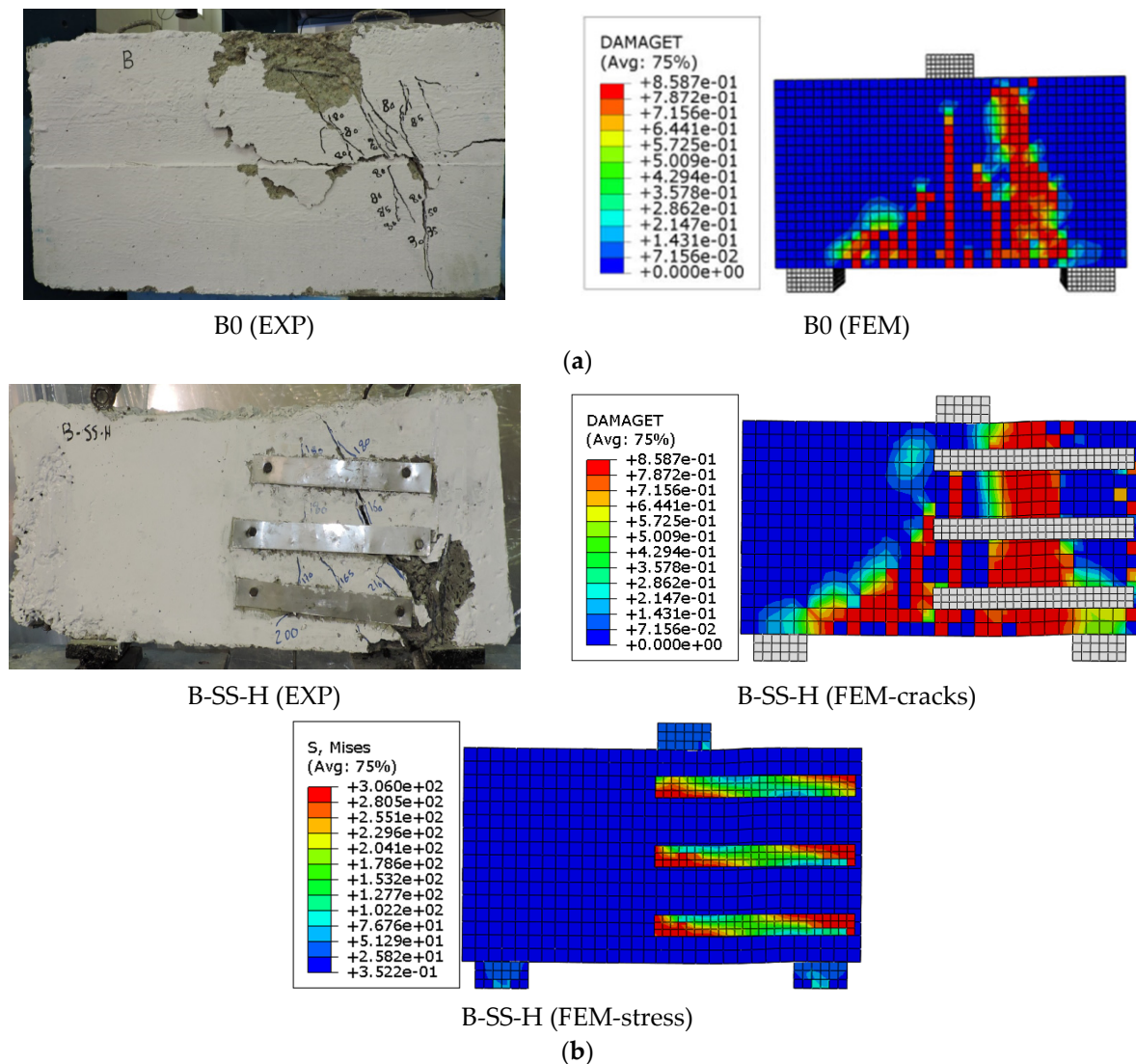


Figure 12. Cont.

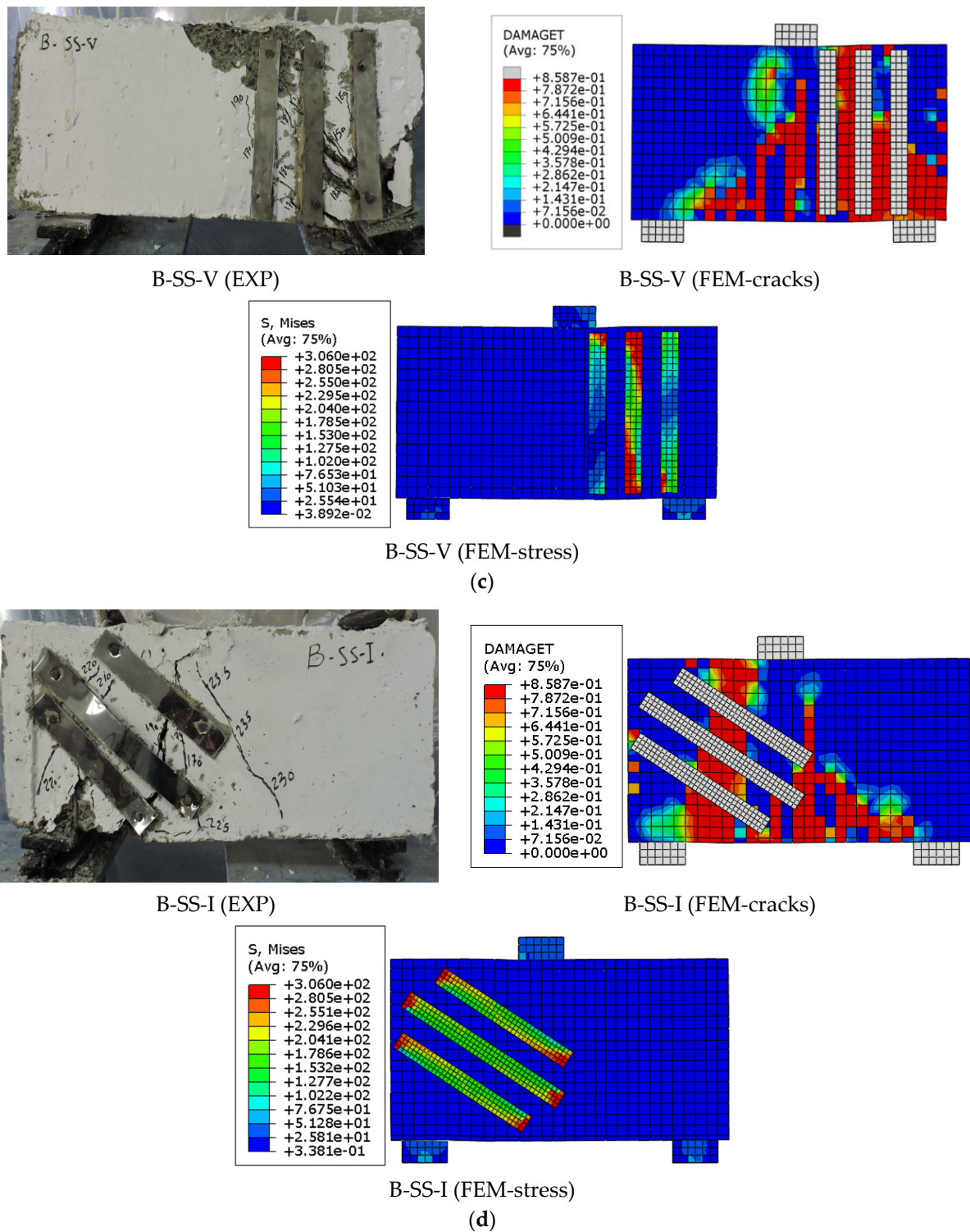


Figure 12. Cracking patterns for test samples and corresponding FE model results.

Table 7. Validating FEM.

Beam's ID	Ultimate Load, $P_u$ (kN)		
	EXP	FEM	FEM/EXP
B0	85	89	0.96
B-SS-H	210	208	1.01

Table 7. Cont.

Beam's ID	Ultimate Load, $P_u$ (kN)		
	EXP	FEM	FEM/EXP
B-SS-V	195	185	1.05
B-SS-I	235	233	1.01
Avg			1.01
SD			0.04
CoV			0.03

Note: EXP: experimental, FEM: finite element modeling.

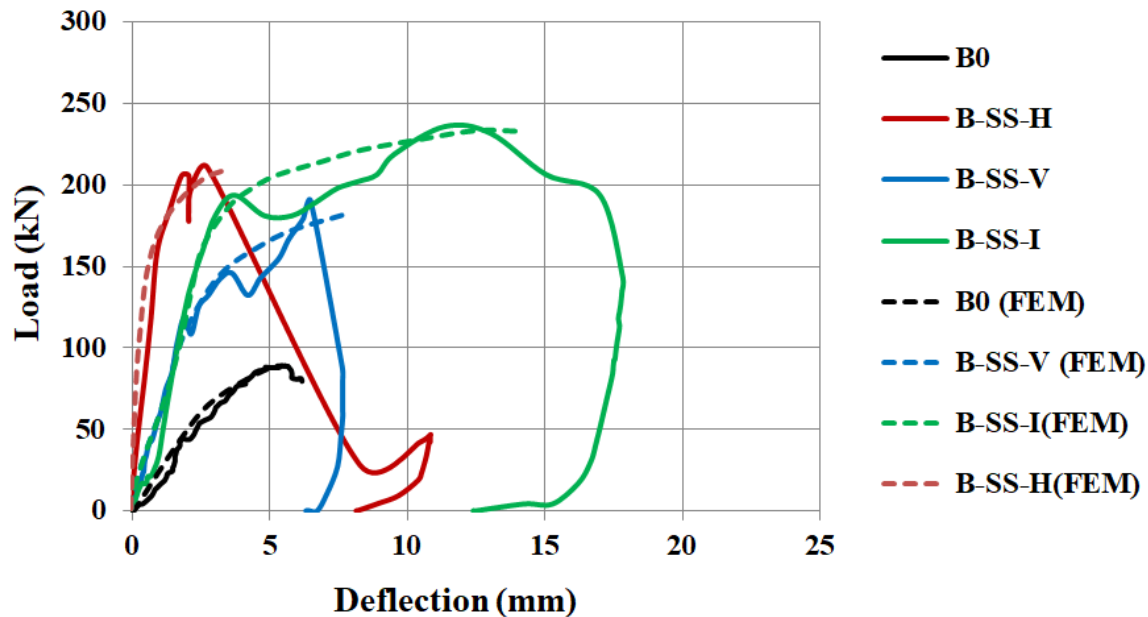


Figure 13. Load–deflection relationships were obtained experimentally and numerically.

## 6. Parametric Study

In this section, the effect of increasing the thickness of the SSPs on the shear stress of the deep beam is examined. The focus is on the deep beam strengthened with inclined strips, as this configuration exhibited the most substantial increase in shear capacity compared to the vertical and horizontal strip orientations. The parametric study aims to study the effects of the thickness of the strips for the most economical benefits as increasing the strip thickness after a critical point may not provide substantial gains in shear strength. The findings of the parametric analysis are shown in Figure 14, which plots the shear stress ( $q_u$ ) versus the ratio of stainless steel area to beam cross-sectional area  $A_{(ss)}\%$ , calculated as follows:

$$A_{(ss)}\% = \frac{A_{ss}}{A_C} \quad (4)$$

where  $A_{ss}$  is the stainless steel area and  $A_C$  is the concrete cross-sectional area.

It is observed that the shear stress increases with increasing the stainless steel plate area up to  $A_{(ss)}\%$  of 0.63%, beyond which the increase in the shear stress remained constant with an increase in plate thickness. Thus, it is proposed to use a maximum of 0.63% of  $A_{(ss)}\%$  for the proposed strengthening technique for practical design purposes.

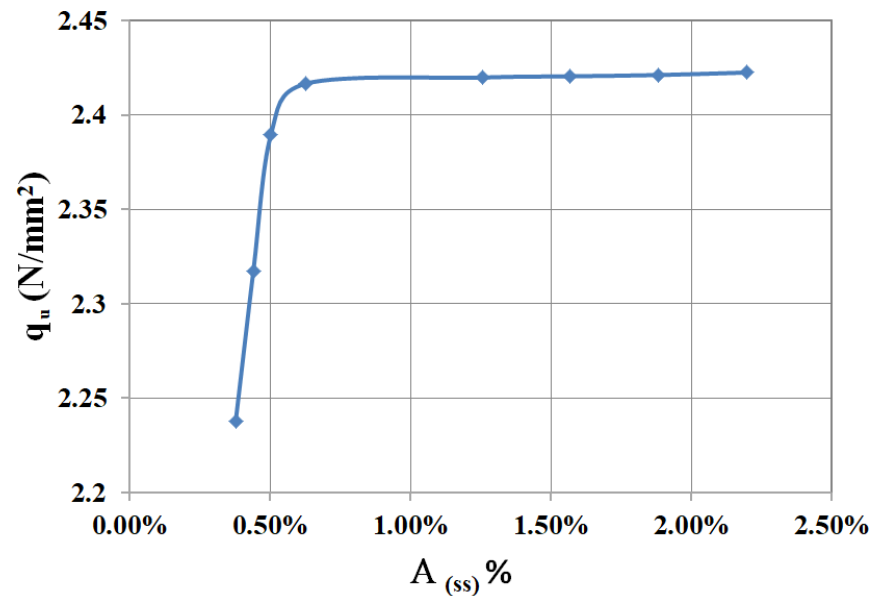


**Figure 14.** Parametric studies with ultimate shear strength versus the ratio of the stainless steel area  $A_{(ss)}$  %.

## 7. Design Code Estimation

In this study, the accuracy of the design equations proposed by Eurocode 2 [31] and ACI-318-19 [32] in predicting the shear strength of the tested beams is examined. It should be noted that the shear strength of the tested beams was calculated based on the zero shear reinforcement ratio, as experimented in this study.

In Eurocode 2 [31], the shear strength for a deep beam without shear reinforcement is calculated as follows:

$$V_c = C_{Rd,c} * b * d \quad (5)$$

where  $C_{Rd,c}$  is a coefficient calculated by Equation (5) based on concrete strength for normal concrete.

$$C_{Rd,c} = 0.12 \sqrt{f'_c} \quad (6)$$

The shear strength of concrete of RC deep beams can be calculated according to ACI-318-19 [32] using Equation (7).

$$V_c = 0.17 \sqrt{f'_c} * b * d \quad (7)$$

Table 8 provides the comparison of the experimental ultimate shear capacity of the tested deep beam with that estimated theoretically according to the code provisions. While EC2 provides an underestimation of the shear strength for the master beam, ACI 318-19 provides an overestimation as can be seen in Table 8. However, it can be seen that the existing design formulas significantly underestimate the ultimate shear strength of the tested deep beams.

**Table 8.** Accuracy of the existing design formulas in predicting the ultimate shear strength of the tested beams.

Beam's ID	EC2			ACI-318-19		
	EXP (kN)	Theo (kN)	Theo/EXP	EXP (kN)	Theo (kN)	Theo/EXP
B0	85	71.8	0.84	85	101.6	1.20
B-SS-H	210	71.8	0.34	210	101.6	0.48
B-SS-V	195	71.8	0.37	195	101.6	0.52
B-SS-I	235	71.8	0.31	235	101.6	0.43

Table 8. Cont.

Beam's ID	EC2			ACI-318-19		
	EXP (kN)	Theo (kN)	Theo/EXP	EXP (kN)	Theo (kN)	Theo/EXP
Avg			0.47			0.66
SD			0.22			0.31
COV			0.47			0.47

## 8. Conclusions

In this study, the performance was examined of shear-strengthened reinforced concrete deep beams using SSPs. The experimental program examines the effects of various configurations of the SSPs on the shear strength of RC deep beams. Numerical modeling simulated the response of SSP-strengthened beams and was validated with test data. A parametric study then investigated the influence of SSP thickness on shear capacity. The accuracy of the design equations given by Eurocode 2 [31] and ACI-318-19 [32] in predicting the shear strength of the deep beams is examined against the test results. The following key conclusions obtained are:

- Unlike the brittle diagonal splitting failure observed in the unstrengthened beam, the inclusion of SSPs promoted a ductile failure mode of deep beams.
- Incorporating SSPs enhanced the ultimate load of the beams in a range of 129%–175%.
- For the beams strengthened with SSPs, positioning of SSPs in inclined positions resulted in the most substantial increase in shear capacity compared to vertical and horizontal strip positionings. Nevertheless, positioning SSPs horizontally exhibited the most increase in the elastic stiffness.
- The developed FEM demonstrated good agreement with experimental data, accurately simulating the load–deflection response, crack patterns, and failure modes of the deep beams strengthened with SSPs. The model captured the distinct behavior of both reinforced and stainless steel-strengthened concrete deep beams. A mean of prediction-to-test cracking and ultimate load ratio of 1.00 and 1.01 was obtained, respectively.
- From the parametric study, it is observed that the increase in the shear strength due to the strengthening of SSPs positioned in an inclined direction became constant as the  $A_{(ss)}$  % reached 0.63% which is proposed to be the maximum adopted for the proposed strengthening technique.
- The existing design formulas given by Eurocode 2 [31] and ACI-318-19 [32] significantly underestimate the ultimate shear strength of the deep beams strengthened using SSPs.
- This study is limited to the shear strengthening of RC deep beams using SSPs. In real life, RC deep beams have openings in the beam's web to facilitate the placement of electrical and mechanical utilities. These openings reduce the beam's load-bearing capacity. Future studies should focus on investigating the performance of shear strengthening of RC deep beams with openings using SSPs. The future study also should develop a design model to calculate the shear strength of RC deep beams using SSPs for practical design applications.

**Author Contributions:** Conceptualization, A.H.; methodology, A.H.; software, A.H., S.A.Y. and R.I.S.; validation, A.H. and S.A.Y.; formal analysis, A.H., S.A.Y. and R.I.S.; investigation, S.A.Y. and R.I.S.; data curation, A.H., S.A.Y., R.I.S. and A.A.A.; writing—original draft, A.H., S.A.Y. and R.I.S.; writing—review and editing, A.A.A., K.S. and M.A.; visualization, S.A.Y., R.I.S., M.A., A.A.A. and K.S.; project administration, A.H. All authors have read and agreed to the published version of the manuscript.

**Funding:** The support through the researchers supporting project (RSP2024R343) provided by King Saud University, Riyadh, Saudi Arabia is acknowledged.

**Data Availability Statement:** The original contributions presented in this study are included in the article; further inquiries can be directed to the corresponding author.

**Acknowledgments:** The technician's help in carrying out the tests at Kafrelsheikh University is acknowledged.

**Conflicts of Interest:** The authors declare no conflicts of interest.

## References

1. Liu, J.; Mihaylov, B. Shear strength of RC deep beams with web openings based on two-parameter kinematic theory. *Struct. Concr.* **2020**, *21*, 349–361. [[CrossRef](#)]
2. Tan, K.-H.; Kong, F.-K.; Teng, S.; Guan, L. High-strength concrete deep beams with effective span and shear span variations. *Struct. J.* **1995**, *92*, 395–405.
3. Rogowsky, D.M.; MacGregor, J.G.; Ong, S.Y. Tests of reinforced concrete deep beams. *J. Proc.* **1986**, *83*, 614–623.
4. Clark, A.P. Diagonal tension in reinforced concrete beams. *J. Proc.* **1951**, *18*, 145–156.
5. Ashour, A. Shear capacity of reinforced concrete deep beams. *J. Struct. Eng.* **2000**, *126*, 1045–1052. [[CrossRef](#)]
6. de Paiva, H.R.; Siess, C.P. Strength and behavior of deep beams in shear. *J. Struct. Div.* **1965**, *91*, 19–41. [[CrossRef](#)]
7. Mau, S.; Hsu, T.S.T. Formula for the shear strength of deep beams. *Struct. J.* **1989**, *86*, 516–523.
8. Mihaylov, B.I.; Bentz, E.C.; Collins, M.P. Two-Parameter Kinematic Theory for Shear Behavior of Deep Beams. *ACI Struct. J.* **2013**, *110*, 447.
9. Russo, G.; Venir, R.; Pauletta, M. Reinforced concrete deep beams-shear strength model and design formula. *ACI Struct. J.* **2005**, *102*, 429.
10. Raheem, M.M. *Structural Behavior of Reinforced Concrete Deep Beams Strengthened in Flexure with CFRP*; Kansas State University: Manhattan, KS, USA, 2019.
11. Hawkins, N.M. *Simplified Shear Design of Structural Concrete Members*; Transportation Research Board: Washington, DC, USA, 2005; Volume 549.
12. Lee, H.-K.; Kim, B.; Ha, S.-K. Numerical evaluation of shear strengthening performance of CFRP sheets/strips and sprayed epoxy coating repair systems. *Compos. Part B Eng.* **2008**, *39*, 851–862. [[CrossRef](#)]
13. Lee, H.-K.; Cheong, S.; Ha, S.-K.; Lee, C. Behavior and performance of RC T-section deep beams externally strengthened in shear with CFRP sheets. *Compos. Struct.* **2011**, *93*, 911–922. [[CrossRef](#)]
14. L'hermite, R. Use of bonding techniques for reinforcing concrete and masonry structures. *Matériaux Constr.* **1977**, *10*, 85–89. [[CrossRef](#)]
15. Ladner, M. Reinforced concrete members with subsequently bonded steel sheets. *IABSE Rep.* **1983**, *46*, 203–210.
16. Täljsten, B. Defining anchor lengths of steel and CFRP plates bonded to concrete. *Int. J. Adhes. Adhes.* **1997**, *17*, 319–327. [[CrossRef](#)]
17. Abdalla, J.A.; Ali, A.B.; Hawileh, R.A.; Mhanna, H.H.; Galal, K.E.; Saqan, E.I. Effect of CFRP anchorages on the flexural behavior of externally strengthened reinforced concrete beams. *Arch. Civ. Mech. Eng.* **2023**, *23*, 242. [[CrossRef](#)]
18. Benaddache, L.; Belkadi, A.A.; Kessal, O.; Berkouche, A.; Noui, A.; Aggoun, S.; Chiker, T.; Tayebi, T. Comparative study on externally bonded heat-treated jute and glass fiber reinforcement for repair of pre-cracked high performance concrete beams. *Arch. Civ. Mech. Eng.* **2024**, *24*, 82. [[CrossRef](#)]
19. Hamoda, A.; Ahmed, M.; Sennah, K. Experimental and numerical investigations of the effectiveness of engineered cementitious composites and stainless steel plates in shear strengthening of reinforced concrete beams. *Struct. Concr.* **2023**, *24*, 2778–2799. [[CrossRef](#)]
20. Bahrami, A.; Ghalla, M.; Elsamak, G.; Badawi, M.; Mlybari, E.A.; Abdelmgeed, F.A. Various configurations of externally bonded strain-hardening cementitious composite reducing shear failure risk of defected RC beams. *Front. Mater.* **2024**, *11*, 1373292. [[CrossRef](#)]
21. Emara, M.; Elsamak, G.; Ghalla, M.; Hu, J.W.; Badawi, M.; Salama, M.I. Shear improvement of defected RC beams with sustainable aluminum boxes incorporating high performance concretes. *Case Stud. Constr. Mater.* **2024**, *21*, e03500. [[CrossRef](#)]
22. Alharthai, M.; Bahrami, A.; Badawi, M.; Ghalla, M.; Elsamak, G.; Abdelmgeed, F.A. Numerical study on enhancing shear performance of RC beams with external aluminum alloy plates bonded using steel anchors. *Results Eng.* **2024**, *22*, 102143. [[CrossRef](#)]
23. Hamoda, A.; Yehia, S.A.; Ahmed, M.; Abadel, A.A.; Baktheer, A.; Shahin, R.I. Experimental and numerical analysis of deep beams with openings strengthened with galvanized corrugated and flat steel sheets. *Case Stud. Constr. Mater.* **2024**, *21*, e03522. [[CrossRef](#)]
24. Hamoda, A.; Ghalla, M.; Yehia, S.A.; Ahmed, M.; Abadel, A.A.; Baktheer, A.; Shahin, R. Experimental and numerical investigations of the shear performance of reinforced concrete deep beams strengthened with hybrid SHCC-mesh. *Case Stud. Constr. Mater.* **2024**, *21*, e03495. [[CrossRef](#)]
25. Akbar, I.; Oehlers, D.J.; Ali, M.M. Derivation of the bond–slip characteristics for FRP plated steel members. *J. Constr. Steel Res.* **2010**, *66*, 1047–1056. [[CrossRef](#)]
26. Biscaia, H.C.; Chastre, C.; Borba, I.S.; Silva, C.; Cruz, D. Experimental evaluation of bonding between CFRP laminates and different structural materials. *J. Compos. Constr.* **2016**, *20*, 04015070. [[CrossRef](#)]

27. Smith, S.T. Strengthening of concrete, metallic and timber construction materials with FRP composites. In *Advances in FRP Composites in Civil Engineering, Proceedings of the 5th International Conference on FRP Composites in Civil Engineering (CICE 2010), Beijing, China, 27–29 September 2010*; Springer: Berlin/Heidelberg, Germany, 2011; pp. 13–19.
28. Abadel, A.A.; Abbas, H.; Almusallam, T.; Alshaikh, I.M.; Khawaji, M.; Alghamdi, H.; Salah, A.A. Experimental study of shear behavior of CFRP strengthened ultra-high-performance fiber-reinforced concrete deep beams. *Case Stud. Constr. Mater.* **2022**, *16*, e011103. [[CrossRef](#)]
29. Ahmad, S.; Elahi, A.; Tufail, R.F.; Zahid, M.; Tariq, S.B. Experimental investigation and strength model of RC deep beams externally bonded by CFRP. *Adv. Struct. Eng.* **2021**, *24*, 3645–3657. [[CrossRef](#)]
30. Biscaia, H.; Franco, N.; Chastre, C. Stainless steel bonded to concrete: An experimental assessment using the DIC technique. *Int. J. Concr. Struct. Mater.* **2018**, *12*, 9. [[CrossRef](#)]
31. *Eurocode 2: Design of Concrete Structures-Part 1-1: General Rules and Rules for Buildings*; European Committee for Standardization (CEN): Brussels, Belgium, 2004.
32. *ACI 318-19; Building Code Requirements for Reinforced Concrete*. American Concrete Institute: Farmington Hills, MI, USA, 2019.
33. *ASTM C39/C39M; Standard Test Method for Compressive Strength of Cylindrical Concrete Specimens*. American Society for Testing and Materials: West Conshohocken, PA, USA, 2021.
34. Hamoda, A.; Abadel, A.A.; Ahmed, M.; Wang, V.; Vrcelj, Z.; Liang, Q.Q. Punching shear performance of reinforced concrete slab-to-steel column connections incorporating ECC and UHPECC. *Eng. Struct.* **2025**, *322*, 119145. [[CrossRef](#)]
35. Ghalla, M.; Badawi, M.; Elsamak, G.; Ahmed, M.; Liang, Q.Q.; El Zareef, M.A. Strengthening of reinforced concrete beams with insufficient lapped splice length of reinforcing bars. *Eng. Struct.* **2024**, *321*, 118922. [[CrossRef](#)]
36. Carreira, D.J.; Chu, K.-H. Stress-strain relationship for plain concrete in compression. *J. Proc.* **1985**, *82*, 797–804.
37. Ahmed, M.; Yehia, S.A.; Shahin, R.I.; Emara, M.; Patel, V.I.; Liang, Q.Q. Numerical analysis of circular steel-reinforced concrete-filled steel tubular stub columns. *Mag. Concr. Res.* **2023**, *76*, 303–318. [[CrossRef](#)]
38. Zheng, Y.; He, C.; Zheng, L. Experimental and numerical investigation of circular double-tube concrete-filled stainless steel tubular columns under cyclic loading. *Thin-Walled Struct.* **2018**, *132*, 151–166. [[CrossRef](#)]

**Disclaimer/Publisher’s Note:** The statements, opinions and data contained in all publications are solely those of the individual author(s) and contributor(s) and not of MDPI and/or the editor(s). MDPI and/or the editor(s) disclaim responsibility for any injury to people or property resulting from any ideas, methods, instructions or products referred to in the content.